Resonance effects on the two-photon emission from hydrogenic ions

P. Amaro,* J. P. Santos,† and F. Parente‡
Departamento de Física, CFA, and Faculdade de Ciências e Tecnologia (FCT), Universidade Nova de Lisboa, 2829-516 Caparica, Portugal

A. Surzhykov§
Physikalisches Institut, Universität Heidelberg, Philosophenweg 12, D-69120 Heidelberg, Germany and GSI Helmholtzzentrum für Schwerionenforschung GmbH, Planckstrasse 1, D-64291 Darmstadt, Germany

P. Indelicato‖
Laboratoire Kastler Brossel, École Normale Supérieure, CNRS, Université Pierre et Marie Curie-Paris 6, Case 74, 4 place Jussieu, 75252 Paris Cedex 05, France

(Received 8 January 2009; revised manuscript received 3 April 2009; published 9 June 2009)

A theoretical study of the all two-photon transitions from initial bound states with $n_i=2,3$ in hydrogenic ions is presented. High-precision values of relativistic decay rates for ions with nuclear charge in the range $1 \leq Z \leq 92$ are obtained through the use of finite basis sets for the Dirac equation constructed from B splines. We also report the spectral (energy) distributions of several resonant transitions, which exhibit interesting structures, such as zeros in the emission spectrum, indicating that two-photon emission is strongly suppressed at certain frequencies. We compare two different approaches (the line profile approach and the QED approach based on the analysis of the relativistic two-loop self-energy) to regularize the resonant contribution to the decay rate. Predictions for the pure two-photon contributions obtained in these approaches are found to be in good numerical agreement.

DOI: 10.1103/PhysRevA.79.062504 PACS number(s): 31.30.J−, 32.70.Fw, 32.80.Wr

I. INTRODUCTION

Two-photon transitions in hydrogen and hydrogenlike ions are under investigation since Göppert-Mayer [1] presented her theoretical formalism in 1931. The early interest in these transitions from metastable states of hydrogen came mainly from astrophysics [2,3], and was recently revived by Chluba and Sunyaev [4]. Among many applications of recent two-photon studies, one can cite the determination of the Rydberg constant [5–7], measurement of the Lamb shift [6,8], and testing Bell's inequality [9], as well as various applications in molecular spectroscopy [10], tissue imaging [11], and protein structure analysis [12]. Another interest in two-photon transitions is connected to the study of parity-violation effects in H-like and He-like ions [13,14]. The two-photon spectral distribution has recently been used for precise efficiency calibration of solid-state x-ray detector as it has a known shape for a large distribution of energies [15].

Similar to single-photon processes, two-photon emission can be spontaneous or stimulated, whereas two-photon absorption is only stimulated. However, since each photon carries one unit of angular momentum in the dipole approximation, certain transitions between atomic energy levels, forbidden as single-photon processes, are allowed as two-photon processes. Another important distinction lies in the fact that the emission spectrum of spontaneous two-photon transitions is continuous unlike the spectrum in a single-photon process. A continuous spectrum is possible because energy conservation requires only that the sum of both photon energies equals the energy of the transition. For the transition

$$(n_i,j_i) \rightarrow (n_f,j_f) + \hbar\omega_1 + \hbar\omega_2, \tag{1}$$

where (n_i,j_i) and (n_f,j_f) denote the principal quantum numbers and total angular momenta of the initial and final hydrogenic states, respectively, and $\hbar\omega_1$ and $\hbar\omega_2$ are the energies of each photon, the conservation of the energy leads to the condition

$$E_i - E_f = \hbar\omega_1 + \hbar\omega_2, \tag{2}$$

where E_i and E_f are the energies of the initial and final ionic states, respectively.

Because of its importance, the $2s_{1/2} \rightarrow 1s_{1/2}$ two-photon transition rate in hydrogen has been calculated and discussed many times using different approaches. A historical overview from both theoretical and experimental points of view can be found in the 1998 paper by Santos *et al.* [16].

Recently, Surzhykov *et al.* [17] performed a relativistic calculation to study the angular correlations in the two-photon decay of hydrogenlike ions, and Labzowsky *et al.* [18] evaluated the $2E1$ contribution for the $2s_{1/2} \rightarrow 1s_{1/2}$ transition and the $E1M1$ and $E1E2$ contributions for the $2p_{1/2} \rightarrow 1s_{1/2}$ transition using an expression similar to the one obtained by Goldman and Drake [19] in the quantum electrodynamics (QED) framework. Also in this framework, Nganso and Njock [20] carried out the treatment of the S matrix for bound-bound transitions.

*p.d.g.amaro@gmail.com
†jps@fct.unl.pt
‡facp@fct.unl.pt
§surz@physi.uni-heidelberg.de
‖paul.indelicato@spectro.jussieu.fr

 ©2009 The American Physical Society

In this work, which uses techniques of a previous one [16], we study the two-photon decay of several excited states using two approaches to deal with resonances, the line profile approach (LPA) [21] and the QED approach based on the analysis of the relativistic two-loop self-energy (TLA), to regularize the resonant contribution to the decay rate [22,23]. We present calculated values for two-photon decay rates obtained with both approaches for one-electron ions with a nuclear charge of up to 92. This paper is organized as follows: in Sec. II we give a brief review of the background theory involved in two-photon emission, in Sec. III we present the results obtained in this work, and the conclusions are presented in Sec. IV.

II. THEORY OF RELATIVISTIC RADIATIVE TRANSITIONS

A. Two-photon spontaneous emission

1. General formalism

The relativistic theory of two-photon transitions is given in detail in Refs. [16,19,24]. In the present work, therefore, we report only the most important equations and notations used.

The basic expression for the differential (in energy of one of the photons) rate is, in atomic units,

$$\frac{dw}{d\omega_1} = \frac{\omega_1\omega_2}{(2\pi)^3 c^2}\left|\sum_\nu \left(\frac{\langle f|A_2^*|\nu\rangle\langle\nu|A_1^*|i\rangle}{E_\nu - E_i + \omega_1} + \frac{\langle f|A_1^*|\nu\rangle\langle\nu|A_2^*|i\rangle}{E_\nu - E_i + \omega_2}\right)\right|^2 d\Omega_1 d\Omega_2, \tag{3}$$

where ω_j is the frequency and $d\Omega_j$ is the element of solid angle of the jth photon, and c is the speed of light. The frequencies of the photons are constrained by energy conservation Eq. (2).

For photon plane wave with propagation vector $\mathbf{k}_j$ and polarization vector $\hat{\boldsymbol{e}}_j$ ($\hat{\boldsymbol{e}}_j \cdot \mathbf{k}_j = 0$), the operators A_j^* in Eq. (3) are given by

$$A_j^* = \boldsymbol{\alpha}\cdot(\hat{\boldsymbol{e}}_j + G\hat{\boldsymbol{k}}_j)e^{-i\mathbf{k}_j\cdot\mathbf{r}} - Ge^{-i\mathbf{k}_j\cdot\mathbf{r}}, \tag{4}$$

where $\boldsymbol{\alpha}$ are Dirac matrices and G is an arbitrary gauge parameter. Among the large variety of possible gauges, Grant [25] showed that there are two values of G which are of particular utility because they lead to well-known nonrelativistic operators. If $G=0$, one has the so-called Coulomb gauge, or velocity gauge, which leads to the dipole velocity form in the nonrelativistic limit. If $G=[(L+1)/L]^{1/2}$, for example, $G=\sqrt{2}$ for $E1$ transitions ($L=1$), one obtains a nonrelativistic expression which reduces to the dipole length form of the transition operator. The two-photon transitions gauge invariance was studied by Goldman and Drake [19]. From the general requirement of gauge invariance the final results must be independent of G.

The index ν stands for all solutions including the discrete and both negative- and positive-energy solutions of the Dirac equation. In Eq. (3), moreover, $|i\rangle = |n_i\kappa_i m_i\rangle$, $|\nu\rangle = |n_\nu\kappa_\nu m_\nu\rangle$, and $|f\rangle = |n_f\kappa_f m_f\rangle$ are the well-known solutions of the Dirac Hamiltonian for a single electron, where n and m stand for the principal quantum number and the one-electron angular momentum projection, respectively. The Dirac quantum number κ is defined by

$$\kappa = \begin{cases} \ell & \text{if } j = \ell - 1/2 \\ -(\ell+1) & \text{if } j = \ell + 1/2, \end{cases} \tag{5}$$

where ℓ and j are the electron orbital and total angular momenta, respectively.

If the energy of an intermediate state E_ν is equal to the energy $E_i - \omega_{1,2}$ in the denominators of Eq. (3), the differential emission rate has a pole or a resonant behavior at E_ν. Physically, this occurs when an intermediate virtual state, between the initial and final states, coincides with a real state so that the two-photon transition coincides with the cascade de-excitation process.

For example, in the $2E1$ $3s_{1/2} \to 1s_{1/2}$ transition, the shape of the frequency distribution presents narrow resonances at energies corresponding to the $3s_{1/2} \to 2p_{1/2,3/2} \to 1s_{1/2}$ cascade. This effect has been confirmed both experimentally [26] and theoretically [27].

The divergent behavior of the resonant denominator in Eq. (3) is related to the Green's function used in that expression, which does not take into account the interaction between the electron and the vacuum fluctuations of the electromagnetic field. The LPA allows derivation of the following expression for the differential emission [21,28], which takes partially into account this contribution:

$$\frac{dw^{\mathrm{LPA}}}{d\omega_1} = \frac{\omega_1\omega_2}{(2\pi)^3 c^2}\left|\sum_\nu \left(\frac{\langle f|A_2^*|\nu\rangle\langle\nu|A_1^*|i\rangle}{V_\nu - V_i + \omega_1} + \frac{\langle f|A_1^*|\nu\rangle\langle\nu|A_2^*|i\rangle}{V_\nu - V_i + \omega_2}\right)\right|^2 d\Omega_1 d\Omega_2, \tag{6}$$

where

$$V_\nu = E_\nu + \eta_\nu\left\{\langle\nu|\sum\nolimits_e|\nu\rangle + \langle\nu|\prod\nolimits_e|\nu\rangle\right\}, \tag{7}$$

with

$$\eta_\nu = \begin{cases} 1 & \text{if } \nu \text{ is a resonant intermediate state} \\ 0 & \text{otherwise,} \end{cases} \tag{8}$$

and $\langle\nu|\Sigma_e|\nu\rangle$ and $\langle\nu|\Pi_e|\nu\rangle$ are the electron mean value of the self-energy (SE) and vacuum polarization (VP) operators in lowest order for the state ν, respectively. Both the mean value of the self-energy and vacuum polarization operators have a real part, ΔE_ν, that is a correction to the energy E_ν. On the other hand, only the self-energy operator has an imaginary part, $\Gamma_\nu/2$, which is the width of the state ν.

The average decay rate, i.e., the decay rate summed over the final m_f and averaged over initial m_i ion magnetic sublevels, can be obtained from Eq. (6) as

$$\frac{dW^{\mathrm{LPA}}}{d\omega_1} = \sum_{L_1,\lambda_1,L_2,\lambda_2} \frac{d\bar{W}^{\mathrm{LPA}}_{L_1,\lambda_1,L_2,\lambda_2}}{d\omega_1}, \tag{9}$$

where the partial decay rates describing the two-photon transitions of a given type (λ) and multipolarity (L) are given by

$$\frac{d\bar{W}^{\mathrm{LPA}}_{L_1,\lambda_1,L_2,\lambda_2}}{d\omega_1} = \frac{\omega_1\omega_2}{(2\pi)^3 c^2(2j_i+1)}\sum_{j_\nu}\Bigg[|\bar{S}^{j_\nu}(2,1)|^2 + |\bar{S}^{j_\nu}(1,2)|^2 + 2\sum_{j_\nu} d(j_\nu,j_\nu)\times\{\mathrm{Re}[\bar{S}^{j_\nu}(2,1)]\mathrm{Re}[\bar{S}^{j_\nu}(1,2)] + \mathrm{Im}[\bar{S}^{j_\nu}(2,1)]\mathrm{Im}[\bar{S}^{j_\nu}(1,2)]\}\Bigg]. \tag{10}$$

Here we define

$$d(j,j') = (-1)^{2j'+L_1+L_2}[j,j']^{1/2}\begin{Bmatrix} j_f & j' & L_1 \\ j_i & j & L_2 \end{Bmatrix}, \tag{11}$$

which represents the angular coupling, and

$$\bar{S}^j(2,1) = \sum_{n_\ell}\frac{\bar{M}^{(\lambda_2,L_2)}_{f,n_\ell}(\omega_2)\bar{M}^{(\lambda_1,L_1)}_{n_\ell,i}(\omega_1)}{V_{n_\ell}-V_i+\omega_1} \times\frac{4\pi[j_i,j,j_f]^{1/2}}{[L_1,L_2]^{1/2}}\pi^\ell_i(1)\pi^\ell_f(2) \times\begin{pmatrix} j_f & L_2 & j \\ \frac{1}{2} & 0 & -\frac{1}{2}\end{pmatrix}\begin{pmatrix} j & L_1 & j_i \\ \frac{1}{2} & 0 & -\frac{1}{2}\end{pmatrix}, \tag{12}$$

with

$$\pi^\ell_k(t) = \begin{cases} 1 & \text{if } \ell_k+\ell+L_t+\lambda_t = \text{odd} \\ 0 & \text{if } \ell_k+\ell+L_t+\lambda_t = \text{even.}\end{cases} \tag{13}$$

$\bar{S}^j(1,2)$ is analogously defined. The notation $[j,k,\ldots]$ means $(2j+1)(2k+1)\cdots$, $(\cdots)$ are the $3j$ symbols, and $\{\cdots\}$ are the $6j$ symbols.

The radial matrix elements $\bar{M}^{(\lambda,L)}_{f,i}$ in Eq. (12) are defined by

$$\bar{M}^{(1,L)}_{f,i} = \left(\frac{L}{L+1}\right)^{1/2}[(\kappa_f-\kappa_i)I^+_{L+1}+(L+1)I^-_{L+1}] - \left(\frac{L+1}{L}\right)^{1/2}[(\kappa_f-\kappa_i)I^+_{L-1}-LI^-_{L-1}], \tag{14}$$

$$\bar{M}^{(0,L)}_{f,i} = \frac{2L+1}{[L(L+1)]^{1/2}}(\kappa_f+\kappa_i)I^+_L, \tag{15}$$

and

$$\bar{M}^{(-1,L)}_{f,i} = G[(2L+1)J^{(L)}+(\kappa_f-\kappa_i)(I^+_{L+1}+I^+_{L-1}) - LI^-_{L-1}+(L+1)I^-_{L+1}]. \tag{16}$$

L is the photon angular momentum and λ stands for the electric ($\lambda=1$), magnetic ($\lambda=0$), and the longitudinal ($\lambda=-1$) terms. We used the notation given by Rosner and Bhalla [29] for the integrals the $I^\pm_L(\omega)$ and $J_L(\omega)$. Parity selection rules (13) follow from the calculation of the reduced matrix elements expressed in Eq. (3).

We emphasize that the term $\pi^\ell_i(1)\pi^\ell_f(2)$ in Eq. (12) is not given explicitly in the paper of Goldman and Drake [19], which could lead to some ambiguity in the choice of the intermediate states for the evaluation of the $\bar{S}^j(2,1)$ and $\bar{S}^j(1,2)$ terms in a generic transition.

Usually, it is convenient to express the results in terms of the electric (E) and magnetic (M) multipole (MP) contributions. The total decay rate (integrated over the photon energy) for a transition in which one photon Θ_1L_1 and one photon Θ_2L_2 are emitted, where $\Theta_i=E,M$ stand for the electric and magnetic multipole types, respectively, is given by

$$\bar{W}^{\mathrm{LPA}}_{\Theta_1L_1\Theta_2L_2} = \sum_{\lambda_{\Theta_1},\lambda_{\Theta_2}}\bar{W}^{\mathrm{LPA}}_{L_1,\lambda_{\Theta_1},L_2,\lambda_{\Theta_2}} = \sum_{\lambda_{\Theta_1},\lambda_{\Theta_2}}\int_0^{\omega_t}\frac{d\bar{W}^{\mathrm{LPA}}_{L_1,\lambda_{\Theta_1},L_2\lambda_{\Theta_2}}}{d\omega_1}d\omega_1, \tag{17}$$

with

$$\lambda_{\Theta_i} = -1,1 \quad \text{if } \Theta_i = E, \qquad \lambda_{\Theta_i} = 0 \quad \text{if } \Theta_i = M, \tag{18}$$

and ω_t is the energy of the two-photon transition, which is given, in a.u., by

$$\omega_t = \omega_1+\omega_2 = E_i - E_f \tag{19}$$

using Eq. (2).

Finally, the total spontaneous emission probability per unit time for a two-photon transition is obtained by summing over all allowed multipole components,

$$W^{\mathrm{LPA}} = \sum_{\text{all }\Theta_1L_1,\Theta_2L_2} t_{\Theta_1L_1,\Theta_2L_2}\bar{W}^{\mathrm{LPA}}_{\Theta_1L_1\Theta_2L_2}, \tag{20}$$

where

$$t_{\Theta_1L_1,\Theta_2L_2} = \begin{cases} 1 & \text{if } \Theta_1L_1 \neq \Theta_2L_2 \\ 1/2 & \text{if } \Theta_1L_1 = \Theta_2L_2.\end{cases} \tag{21}$$

The factor of 1/2 is included to avoid counting twice each pair, when both photons have the same characteristics.

Another method for dealing with resonances was developed by Jentschura and Surzhykov [22,23] using a procedure based on TLA. They obtained an expression similar to Eq. (3) for evaluating a nonresonant component of the two-photon decay rate, given by

$$w^{\mathrm{TLA}} = \lim_{\epsilon\to 0}\mathrm{Re}\int_0^{\omega_t} d\omega_1\frac{\omega_1\omega_2}{(2\pi)^3c^2}\mathcal{S}_{ij}d\Omega_1 d\Omega_2. \tag{22}$$

The function $\mathcal{S}_{if}$ is given, as in Ref. [23], by

$$\mathcal{S}_{if} = \left(\sum_\nu\left\{\frac{\langle f|A^*_2|\nu\rangle\langle\nu|A^*_1|i\rangle}{E_\nu-E_i+\omega_1-i\epsilon}+\frac{\langle f|A^*_1|\nu\rangle\langle\nu|A^*_2|i\rangle}{E_\nu-E_i+\omega_2-i\epsilon}\right\}\right)^2. \tag{23}$$

Using this approach one obtains finite results since the integration over the frequency ω_1 is displaced by an infini-

tesimal quantity, ϵ, from the resonance poles, provided the limit is not permuted with the integration.

If one considers a nonresonant transition such as $2s_{1/2} \rightarrow 1s_{1/2}$, then the limit can be permuted with the integration and Eq. (22) reduces to Eq. (3), and both approaches give the same result.

2. Integration method for resonant intermediate states

For resonant transitions, Eq. (10) produces sharp peaks near the resonant frequencies, which requires special attention in the integration over the photon energy ω_1 in Eq. (17) to avoid meaningless results for the total decay rate. Near a resonant frequency $\omega_R^{j_\nu}$, Eq. (10) can be written as

$$\frac{d\bar{W}^{\mathrm{LPA}}_{L_1,\lambda_1,L_2,\lambda_2}}{d\omega_1} = \sum_{j_\nu} g^{j_\nu}(\omega_1) = \sum_{j_\nu} \frac{f^j(\omega_1)}{(\omega_1 - \omega_R^{j_\nu})^2 + \left(\frac{\Gamma_R^{j_\nu}}{2}\right)^2}, \tag{24}$$

where $f^j(\omega_1)$ is a smooth function; the resonant behavior is given by the denominator. Consequently, the function $f^j(\omega_1)$ can be expanded in a Taylor series around the resonant frequency $\omega_R^{j_\nu}$. Notice that the shape in the right-hand side of Eq. (24) is not a Lorentz profile since $f^j(\omega_1)$ depends on ω_1, and so the peak profile is asymmetric. Subtracting the first two terms of the expansion on $g^j(\omega_1)$ we obtain a smooth function, $h^{\mathrm{LPA}}(\omega_1)$, which does not contain a resonant behavior. It is defined as

$$h^{\mathrm{LPA}}(\omega_1) = \sum_{j_\nu} \left[g^{j_\nu}(\omega_1) - \frac{a_0^{j_\nu}}{(\omega_1 - \omega_R^{j_\nu})^2 + \left(\frac{\Gamma_R^{j_\nu}}{2}\right)^2} - \frac{a_1^{j_\nu}(\omega_1 - \omega_R^{j_\nu})}{(\omega_1 - \omega_R^{j_\nu})^2 + \left(\frac{\Gamma_R^{j_\nu}}{2}\right)^2} \right]. \tag{25}$$

The coefficients a_0^j and a_1^j are derived from the Taylor expansion of $f^j(\omega_1)$ around ω_R:

$$a_0^j = f^j(\omega_R) = g^j(\omega_R)\left(\frac{\Gamma_R^j}{2}\right)^2,$$

$$a_1^j = \left\{\frac{d}{d\omega_1} f^j(\omega_1)\right\}_{\omega_R} = \left\{\frac{d}{d\omega_1} g^j(\omega_1)\right\}_{\omega_R} \left(\frac{\Gamma_R^j}{2}\right)^2. \tag{26}$$

The expressions of the derivatives of the matrix elements used to evaluate a_1^j are presented in the Appendix.

To obtain the decay rate $\bar{W}^{\mathrm{LPA}}_{L_1,\lambda_1,L_2,\lambda_2}$, we must add to the integral of the smooth function h^{LPA} the two terms $\mathfrak{h}_0^{\mathrm{LPA}}$ and $\mathfrak{h}_1^{\mathrm{LPA}}$ evaluated analytically, i.e.,

$$\bar{W}^{\mathrm{LPA}}_{L_1,\lambda_1,L_2,\lambda_2} = \mathfrak{h}^{\mathrm{LPA}} + \mathfrak{h}_0^{\mathrm{LPA}} + \mathfrak{h}_1^{\mathrm{LPA}}, \tag{27}$$

where

$$\mathfrak{h}^{\mathrm{LPA}} = \int_0^{\omega_t} h^{\mathrm{LPA}} d\omega_1, \tag{28}$$

$$\mathfrak{h}_0^{\mathrm{LPA}} = \sum_{j_\nu} a_0^{j_\nu} \int_0^{\omega_t} \frac{1}{\left|\omega_1 - \omega_R^{j_\nu} - i\frac{\Gamma_R^{j_\nu}}{2}\right|^2} d\omega_1 = \sum_j \frac{2a_0^{j_\nu}}{\Gamma_R^j} \arctan\left(\frac{2(\omega_1 - \omega_R^{j_\nu})}{\Gamma_R^{j_\nu}}\right)\Bigg|_0^{\omega_t}, \tag{29}$$

$$\mathfrak{h}_1^{\mathrm{LPA}} = \sum_{j_\nu} a_1^{j_\nu} \int_0^{\omega_t} \frac{(\omega_1 - \omega_R^{j_\nu})}{\left|\omega_1 - \omega_R^{j_\nu} - i\frac{\Gamma_R^{j_\nu}}{2}\right|^2} d\omega_1 = \sum_j \frac{a_1^{j_\nu}}{2} \ln\left[\frac{(\omega_t - \omega_R^{j_\nu})^2 + (\Gamma_R^{j_\nu}/2)^2}{(\omega_R^{j_\nu})^2 + (\Gamma_R^{j_\nu}/2)^2}\right]. \tag{30}$$

We note that a_0^j is given approximately (unless we consider the limit $\Gamma \rightarrow 0$, in which case it is given exactly) as

$$a_0^j \approx \frac{w_{i\rightarrow r}^{\lambda_2,L_2} w_{r\rightarrow f}^{\lambda_1,L_1}}{2\pi}, \tag{31}$$

where the term $w_{i\rightarrow f}^{\lambda_k,L_k}(\omega)$ is the decay rate from an initial to a final state through the emission of one photon, which is given, in a.u., by [25]

$$w_{i\rightarrow f}^{\lambda L}(\omega) = \frac{2\omega[j_f]}{c[L]} \begin{pmatrix} j_f & L & j_i \\ \frac{1}{2} & 0 & -\frac{1}{2} \end{pmatrix}^2 |\bar{M}_{f,i}^{\lambda L}|^2. \tag{32}$$

Using this result we can write the term

$$\frac{d\mathfrak{h}_0^{\mathrm{LPA}}}{d\omega_1} \approx \sum_{j_\nu} \frac{1}{2\pi} \frac{w_{i\rightarrow r} w_{r\rightarrow f}}{(\omega_1 - \omega_R^{j_\nu})^2 + \left(\frac{\Gamma_R^{j_\nu}}{2}\right)^2}, \tag{33}$$

and identify $\mathfrak{h}_0^{\mathrm{LPA}}$ as a cascade transition rate contribution.

Applying a similar approach to w^{TLA} given by Eq. (22), we obtain a smooth function h^{TLA} as in the LPA. One difference between the two approaches is in the term of order $\sim(\Gamma_R/2)^2$, which appears in the denominator of Eq. (25) and results from considering the infinitesimal quantity ε as finite, i.e., taking the role of a level width ($\epsilon \rightarrow \Gamma$). In the present evaluation we obtain the function h^{TLA} by replacing $\Gamma_R \rightarrow q\Gamma_R$, where q is a parameter that can be made arbitrarily small. We thus obtain convergence since the difference in h^{TLA} using $q=1$ or $q=10^{-2}$ is in the fifth digit. For $q=10^{-2}$ and $q=10^{-3}$ the difference in h^{TLA} is in the ninth digit. So we conclude that using h^{LPA} defined in Eq. (25) with $q=10^{-2}$ is a good approximation for the function h^{TLA}. Another difference between TLA and LPA is the inclusion of radiative corrections Re[SE] and VP, which for values of Z as high as 92 changes the value of h from one approach to another in the second digit. The major difference between the two approaches is in the integral $\mathfrak{h}_0$, which in TLA is given by

$$\mathfrak{h}_0^{\mathrm{TLA}} = \sum_{j_\nu} a_0^{j_\nu} \frac{1}{\omega_R^{j_\nu}(\omega_R^{j_\nu} - \omega_t)}, \tag{34}$$

which comes from the different ways the pole regularization is done.

Notice that the terms $\mathfrak{h}_0^{\mathrm{LPA}}$ and $\mathfrak{h}_0^{\mathrm{TLA}}$ are related by

$$\mathfrak{h}_0^{\mathrm{LPA}} = \mathfrak{h}_0^{\mathrm{TLA}} + \sum_{j_\nu} \frac{2\pi a_0^{j_\nu}}{\Gamma_R^{j_\nu}} + O(\Gamma_R^{j_\nu}), \tag{35}$$

which shows that the difference between $\mathfrak{h}_0^{\mathrm{LPA}}$ and $\mathfrak{h}_0^{\mathrm{TLA}}$ is mainly due to the second term on the left side of Eq. (35) (since $\Gamma_R^j \ll 1$) or by the product of one-photon transitions (cascade process).

On the other hand, the integral $\mathfrak{h}_1$ is given in the TLA approach by

$$\mathfrak{h}_1^{\mathrm{TLA}} = \sum_{j_\nu} a_1^{j_\nu} \ln\left[\frac{\omega_t - \omega_R^{j_\nu}}{\omega_R^j}\right]. \tag{36}$$

This expression can be obtained from Eq. (30) by taking $\Gamma_R \to 0$.

Considering that

$$\mathfrak{h}^{\mathrm{TLA}} = \int_0^{\omega_t} h^{\mathrm{TLA}} d\omega_1, \tag{37}$$

the decay rate in the TLA, $\bar{W}^{\mathrm{TLA}}_{L_1,\lambda_1,L_2,\lambda_2}$, is given by an expression similar to Eq. (27), in which the LPA contributions are replaced by the corresponding TLA contributions.

As we will see in Sec. III, these differences on the sum of $\mathfrak{h}$ and $\mathfrak{h}_1$ do not carry any sizable difference between the LPA and TLA methods for low-Z ions, but lead to slight discrepancy for heavier systems.

B. Solution of the Dirac-Fock equation on a B-spline basis set

To make the numerical evaluation we consider that the atom, or ion, is enclosed in a finite cavity with a radius large enough to get a good approximation of the wave functions, with some suitable set of boundary conditions, which allows for discretization of the continua.

Let us denote by $\{\phi_n^i(r), i=1,\ldots,2N\}$ a set of solutions of the Dirac-Fock equation, where n is the level, i the position of the solution in the set, and N is the number of functions in the basis set.

For each n value the set is complete, and $\phi_n^i(r)$ obeys the equation [30]

$$\begin{bmatrix} \frac{V(r)}{c} & \frac{d}{dr} - \frac{\kappa}{R} \\ -\left(\frac{d}{dr} + \frac{\kappa}{R}\right) & -2c + \frac{V(r)}{c} \end{bmatrix} \phi_n^i(r) = \frac{\varepsilon_n^i}{c} \phi_n^i(r), \tag{38}$$

where the energy E_n^i was replaced by $\epsilon_n^i = E_n^i - mc^2$. The potential $V(r)$ is given by a Coulomb potential assuming a uniform nuclear charge distribution for a finite nucleus and κ is given by Eq. (5). A complete set spans both positive and negative solutions. Solutions labeled by $i=1,\ldots,N$ describe the continuum $\varepsilon_n^i < -2mc^2$ and solutions labeled by $i=N+1,\ldots,2N$ describe bound states (the few first ones) and the continuum $\varepsilon_n^i > 0$. For practical reasons, such as easy numerical implementation, this set of solutions is itself expressed as linear combination of another basis set. We have chosen the B-spline basis set and we used the derivation of the solution of Eq. (38) in terms of B splines described by Johnson *et al.* [31].

TABLE I. MP contributions included in the present calculation of the total two-photon rate for the $2p_{1/2} \to 1s_{1/2}$ transition and comparison between the values obtained in this work [Eq. (17)] and other theoretical values.

	Contribution (s^{-1})		
MP	$Z=1$	$Z=40$	$Z=92$
$E1M1$	9.676654×10^{-6}	6.027323×10^{7}	3.863302×10^{10}
	9.667×10^{-6} [a]	6.020×10^{7} [a]	3.859×10^{10} [a]
	9.677×10^{-6} [b]	6.341×10^{7} [b]	4.966×10^{10} [b]
$E1E2$	6.61179×10^{-6}	4.092020×10^{7}	2.358404×10^{10}
	6.605×10^{-6} [a]	4.088×10^{7} [a]	2.357×10^{10} [a]
	6.673×10^{-6} [b]	4.374×10^{7} [b]	3.425×10^{10} [b]
$M1M2$	3.827877×10^{-17}	5.602320×10^{2}	7.689142×10^{6}
$E2M2$	9.385470×10^{-17}	1.521687×10^{3}	2.834065×10^{7}
$E2E3$	4.095985×10^{-18}	6.608612×10^{1}	1.177403×10^{6}
Total	1.628845×10^{-5}	1.01195×10^{8}	6.225309×10^{10}

[a] Labzowsky *et al.* [18].
[b] Labzowsky *et al.* [32].

III. NUMERICAL RESULTS AND DISCUSSION

By taking $\eta_\nu = 0$ in Eq. (7) we may calculate the two-photon decay rates without accounting for radiative corrections. In this case, we have verified with respect to variations in the gauge parameter ($G=0$ for velocity gauge and $G=\sqrt{2}$ for length gauge), the radius of the cavity (R), and the basis-set parameters [the number (ns) and the degree (k) of the B splines], the stability and accuracy to six digits on the calculation of Eq. (10) for a nonresonant states and for a frequency ω_1.

The parameters used in the calculation of the results presented in this work are $k=9$, $ns=60$, and $R=60$ a.u.. The integration over the photon frequency has been performed using a 15-point Gauss-Legendre algorithm for the nonresonant transitions.

A. Nonresonant transitions

For the nonresonant $2s_{1/2} \to 1s_{1/2}$ and $2p_{1/2} \to 1s_{1/2}$ transitions, we use Eq. (9) for both the decay rate values for various multipole combinations $(\Theta_1 L_1, \Theta_2 L_2)$ and the frequency distribution.

The most significant multipole combinations included in the calculation of the two-photon decay rates of the $2p_{1/2} \to 1s_{1/2}$ transition are presented in Table I. The magnitudes of the multipole combinations not listed in this table are, at least, 4 orders of magnitude smaller than the most significant $E1M1$ and $E1E2$ decay channels.

The values given by Labzowsky *et al.* in [18] were obtained using expressions similar to the ones used by Goldman and Drake [19]. In Ref. [32], the results were obtained using nonrelativistic Coulomb Green's function, which for

TABLE II. Total two-photon decay rates (s^{-1}) for the transitions $2s_{1/2} \rightarrow 1s_{1/2}$ and $2p_{1/2} \rightarrow 1s_{1/2}$ and comparison between the values obtained in this work [Eq. (20)] and other theoretical values.

Total decay rate (s^{-1})		
	$Z=1$	
	i	
f	$2s_{1/2}$	$2p_{1/2}$
$1s_{1/2}$	8.229059	1.628845×10^{-5}
	8.2202[a]	1.6272×10^{-5} [a]
		1.6350×10^{-5} [b]
	$Z=40$	
	i	
f	$2s_{1/2}$	$2p_{1/2}$
$1s_{1/2}$	3.198851×10^{10}	1.01195×10^{8}
	3.1954×10^{10} [a]	1.010×10^{8} [a]
		1.071×10^{8} [b]
	$Z=92$	
	i	
f	$2s_{1/2}$	$2p_{1/2}$
$1s_{1/2}$	3.835978×10^{12}	6.225309×10^{10}
	3.8216×10^{12} [a]	6.216×10^{10} [a]
		8.391×10^{10} [b]

[a]Labzowsky *et al.* [18].
[b]Labzowsky *et al.* [32].

high values of Z such as 92 leads to inaccurate values. The relative difference between our results and the results in Ref. [18] is in the range of 0.1–0.4 %. We observe that for the three studied Z values, more than 99% of the total decay rate is due to the multipole contributions $E1M1$ (about 60%) and $E1E2$ (about 40%). The fact that the two multipole combinations $E1M1$ and $E1E2$ give almost the same contribution is somewhat expected since $M1$ and $E2$ have the same order of magnitude in the decomposition of the photon field [24]. On the other hand, a comparison between the listed most significant ($E1M1$) and less ($E2E3$) significant contributions reveals that the relative importance of the latter increases with Z, being 12, 5, and 4 orders of magnitude smaller than the former for $Z=1$, $Z=40$, and $Z=92$, respectively.

In Table II, we report the two-photon total decay rates for $2p_{1/2} \rightarrow 1s_{1/2}$ and $2s_{1/2} \rightarrow 1s_{1/2}$ transitions. Enough multipoles have been included in the calculation of the total two-photon decay rates to reach an accuracy of six digits. The values for the $2s_{1/2} \rightarrow 1s_{1/2}$ transition differ slightly from the ones in our previous work [16] due to use of the most recent values of physical constants [33], such as the fine-structure constant.

It should be mentioned that the interest in the transition $2p_{1/2} \rightarrow 1s_{1/2}$, and other two-photon-forbidden transitions, is only academic since the transition is suppressed by selection rules and this channel is in direct competition with an allowed one-photon transition.

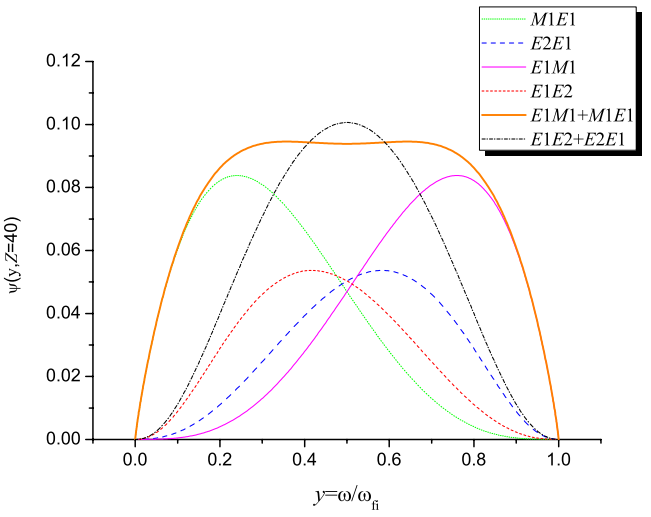

FIG. 1. (Color online) Spectral distribution functions $\psi(y,Z)$, defined by Eq. (39), of the $M1E1$ (dotted line), $E2E1$ (long-dashed line), $E1M1$ (thin solid line), $E1E2$ (short-dashed line), $M1E1+E1M1$ (thick solid line), and $E2E1+E1E2$ (dash-dotted line) contributions for the transition $2p_{1/2} \rightarrow 1s_{1/2}$ at $Z=40$. The variable $y=\omega/\omega_{fi}$ is the fraction of the photon energy carried by one of the two photons. Both $\psi(y,Z)$ and y are dimensionless quantities.

To present the spectral (or frequency) distribution for a specific value of Z, it is convenient to express the results in $\psi(y,Z)$ as suggested by Spitzer and Greenstein [2],

$$\frac{dW}{dy} = \left(\frac{9}{2^{10}}\right)(Z\alpha)^n \psi(y,Z)\ \mathrm{Ry}, \tag{39}$$

where $y=\omega/\omega_{fi}$ is the fraction of the photon energy carried by one of the photons and ω_{fi} is the energy of the transition. In case of an even $\rightarrow$ even (or odd $\rightarrow$ odd) transition, the major multipole contribution $2E1$ scales as Z^6 and, consequently, $n=6$. For a even $\rightarrow$ odd (or odd $\rightarrow$ even) transition, both $E1M1$ and $E1E2$ scale as Z^8.

In Fig. 1, the frequency distributions of the multipole contributions $E1M1$, $M1E1$, $E1E2$, and $E2E1$ for the transition $2p_{1/2} \rightarrow 1s_{1/2}$ are presented. Although each one of these four most significant contributions is asymmetric, the sum of each of the pairs $(E1M1, M1E1)$ and $(E1E2, E2E1)$ is symmetric around $y=0.5$. Therefore, the total frequency distribution is also symmetric around the $y=0.5$ value, as can be seen in Fig. 2, in which we also notice the Z dependence of the shape predicted by Goldman and Drake [19] for the $2s_{1/2}$-$1s_{1/2}$ transition.

B. Resonant transitions

After this brief discussion of the nonresonant $2s_{1/2} \rightarrow 1s_{1/2}$ and $2p_{1/2} \rightarrow 1s_{1/2}$ two-photon transitions, we now turn to the evaluation of the differential total decay rates for the higher excited ionic states. In Fig. 3, for example, we display the spectral distribution for the $3s_{1/2} \rightarrow 1s_{1/2}$ transition. We notice several features that are not found in the corresponding plot for the $2s_{1/2} \rightarrow 1s_{1/2}$ transition. In particu-

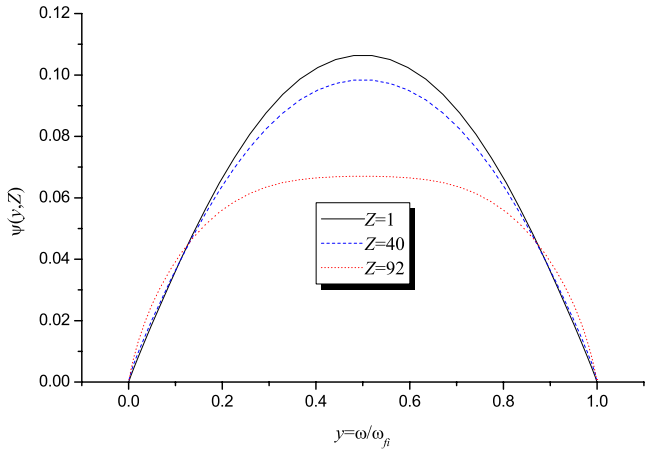

FIG. 2. (Color online) Spectral distribution functions $\psi(y,Z)$, defined by Eq. (39), for the transition $2p_{1/2}\rightarrow 1s_{1/2}$ at $Z=1$ (solid line), 40 (dashed line), and 92 (dotted line). The variable $y=\omega/\omega_{fi}$ is the fraction of the photon energy carried by one of the two photons. Both $\psi(y,Z)$ and y are dimensionless quantities.

lar, the $\psi_{3s_{1/2}\rightarrow 1s_{1/2}}(y,Z)$ function exhibits sharp peaks, which are due to the $3s_{1/2}\rightarrow 2p_{1/2,3/2}\rightarrow 1s_{1/2}$ cascade. Furthermore, we observe that at $Z=92$ each of the two resonances splits into two due to the spin-orbit interaction and the frequency gap in each pair is exactly equal to the difference between the states $2p_{3/2}$ and $2p_{1/2}$, respectively. In addition, besides the zeros at the end points, there are two more minima at $y=0.219\,733$ and $0.780\,267$. Such minima were observed in two-photon spectra by Tung *et al.* [34,35], and they were referred to as "transparencies." In Table III we list the transparencies for several two-photon transitions obtained in this work by other authors. Their relative differences are smaller than 0.01% for $Z=1$. To the best of our knowledge, there are no published data for other Z values. In Fig. 4 we plot the transparency frequency y^{transp} of the transition $3s_{1/2}\rightarrow 1s_{1/2}$ as function of Z. We notice that the transparency values scale with Z^2 as the transition energy.

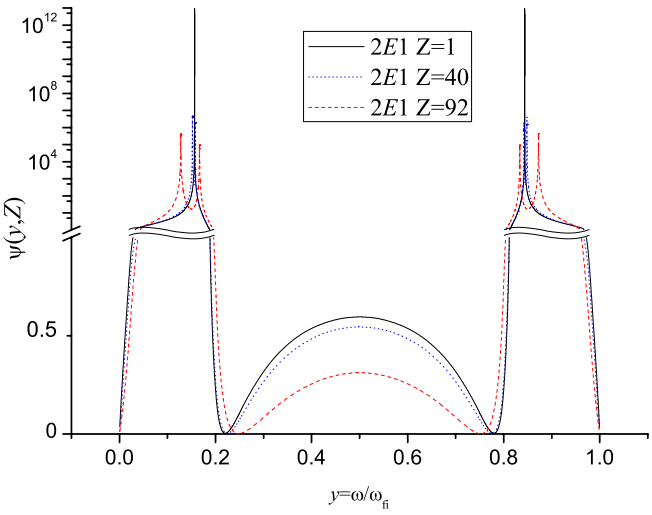

FIG. 3. (Color online) Spectral distribution functions $\psi(y,Z)$, defined by Eq. (39), of the $2E1$ contribution for the transition $3s_{1/2}\rightarrow 1s_{1/2}$ at $Z=1$ (solid line), 40 (dotted line), and 92 (dashed line). The variable $y=\omega/\omega_{fi}$ is the fraction of the photon energy carried by one of the two photons. Both $\psi(y,Z)$ and y are dimensionless quantities.

TABLE III. Transparencies for several two-photon transitions. The variable $y=\omega_1/\omega_{fi}$ is the fraction of the photon energy carried by one of the two photons.

Transition	$y(Z=1)$	$y(Z=40)$	$y(Z=92)$
$3s_{1/2}\rightarrow 1s_{1/2}$	0.780267	0.77628	0.7518
	0.7803[a]		
	0.7802[b]		
	0.7803[c]		
$4s_{1/2}\rightarrow 1s_{1/2}$	0.737322	0.73273	0.7034
	0.7373[a]		
	0.7373[c]		
$6s_{1/2}\rightarrow 1s_{1/2}$	0.703220	0.70497	0.6725
	0.7098[a]		
	0.7079[b]		
	0.7098[c]		

[a]Florescu *et al.* [44].
[b]Quattropani *et al.* [45].
[c]Tung *et al.* [34].

In contrast to the $3s_{1/2}\rightarrow 1s_{1/2}$, the spectral distribution for the $3d_{3/2}\rightarrow 1s_{1/2}$ transition, plotted in Fig. 5, exhibits only the resonant behavior as mentioned in Ref. [34], which is due to the fine-structure splittings between $2p_{1/2}$ and $2p_{3/2}$ and $3p_{1/2}$ and $3d_{3/2}$ states.

In Fig. 6, we plot the frequency distribution of the multipole $E1M1$ contribution for the $2p_{3/2}\rightarrow 1s_{1/2}$ transition. Along with the resonances, the shape of the curve is similar to the one in Fig. 1 for the $2p_{1/2}\rightarrow 1s_{1/2}$ transition. In the $E1M1$ case, the resonance in the low-frequency side occurs when the energy of one of the photons is equal to the energy difference $E_{2p_{3/2}}-E_{2s_{1/2}}$, while the resonance in the high-frequency side occurs when the energy of one of the photons is equal to the energy difference $E_{2p_{3/2}}-E_{2p_{1/2}}$.

The list of the radiative corrections contributions for some states, which were included in Eq. (12) to achieve an accu-

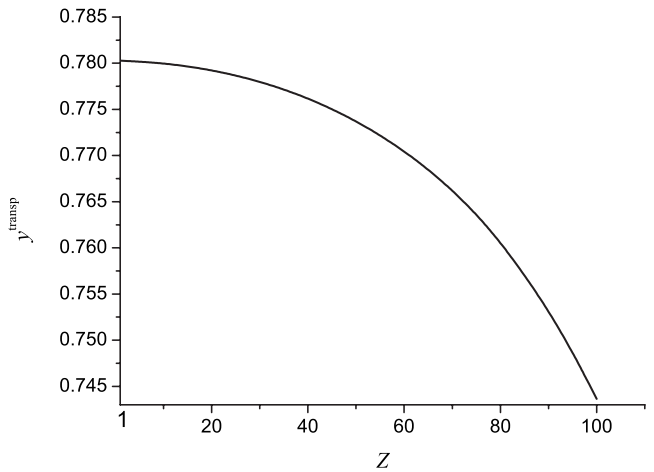

FIG. 4. Transparency frequency y^{transp} of the transition $3s_{1/2}\rightarrow 1s_{1/2}$ as function of the atomic number Z.

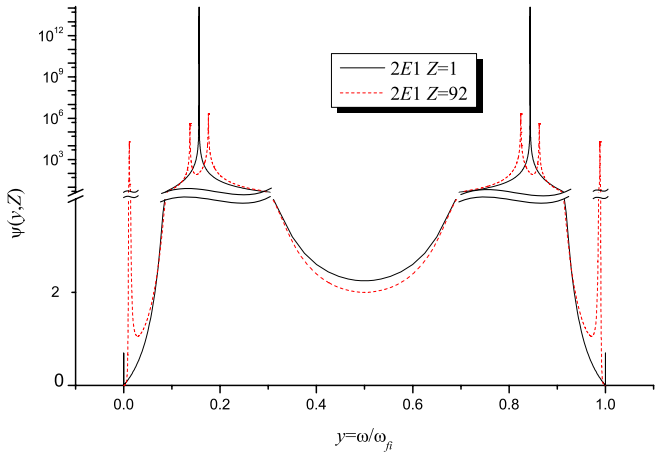

FIG. 5. (Color online) Spectral distribution functions $\psi(y,Z)$, defined by Eq. (39), of the $2E1$ contribution for the transition $3d_{3/2} \rightarrow 1s_{1/2}$ at $Z=1$ and 92. For the legend, see Fig. 3 caption.

racy of at least six digits, is included in Table IV. The values for the real part of self-energy and vacuum polarization were obtained from the MCDF code developed by Desclaux , Indelicato, and collaborators [36–38]. The level width Γ_ν is equal to the sum of the one-photon partial level widths, given by Eq. (32).

As seen from Eq. (17), by performing the integration of the differential transition probabilities over energy of the emitted photon, we may finally obtain the total two-photon decay rates. Equation (27) shows that these rates can be traced back to $\mathfrak{h}$ functions. In Table V, we list the sums of the terms $\mathfrak{h}^{\mathrm{LPA}}$ and $\mathfrak{h}_1^{\mathrm{LPA}}$ given by Eqs. (28) and (30), required for the evaluation of the decay rates for transitions from bound states with $n_i=3$ in the LPA, including the most relevant multipoles, radiative corrections, and using $q=1$. The corresponding values obtained in TLA are listed in Table VI. By comparing the values in these two tables, we conclude that they differ less than 0.001% for $Z=1$, 2.3% for $Z=40$, and 10% for $Z=92$, which shows the importance of the radiative effects.

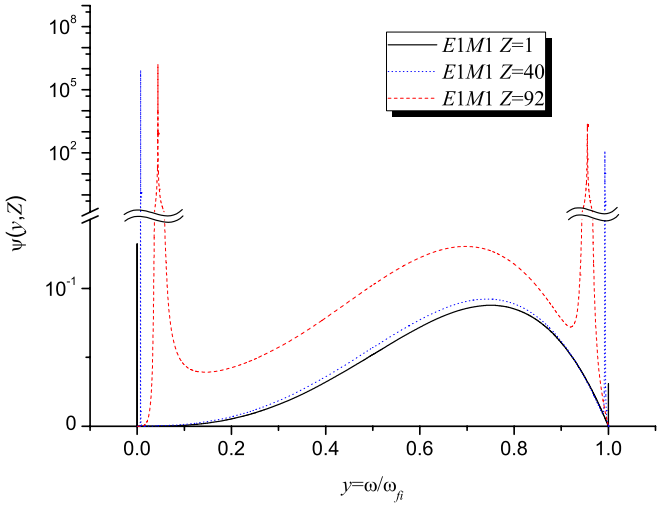

FIG. 6. (Color online) Spectral distribution functions $\psi(y,Z)$, defined by Eq. (39), of the $E1M1$ contribution for the transition $2p_{3/2} \rightarrow 1s_{1/2}$ at $Z=1$, 40, and 92. For the legend, see Fig. 3 caption.

In Tables VII and VIII, we list the most relevant multipole combinations included in the calculation of the two-photon decay rate for the $2p_{3/2} \rightarrow 1s_{1/2}$ and $3s_{1/2} \rightarrow 2s_{1/2}$ transitions. We notice that for $Z=1$ the decay rate values of some multipole contributions, such as the $E1M1$ and the $E1E2$, listed in Table VII, are similar to the corresponding ones for the transition $2p_{1/2} \rightarrow 1s_{1/2}$. Nevertheless, this is not the case for $Z=40$ and $Z=92$. This is due to the fact that the energy separation between $2p_{3/2}$ and $2s_{1/2}$ increases with Z and, consequently, the decay rate contribution from the cascade process also increases. This aspect is also evident in Fig. 7, where the multipole combination $E1M1$ decay rate W_{E1M1}, obtained in the LPA and TLA, is plotted as a function of the atomic number Z for the $2p_{1/2,3/2} \rightarrow 1s_{1/2}$ transitions.

The resonant behavior of the $2p_{3/2} \rightarrow 1s_{1/2}$ transition is strongly suppressed for low Z values. We notice that for lower Z values both solid (LPA) and dotted (TLA) lines have similar values, which is a consequence of the fact that nonresonant contribution (related to integral of "background") in both transitions (M1E1 in Figs. 1 and 6) is much higher than the cascade term (dashed line). For higher values of Z, we notice that the solid line follows the dashed line. This could be explained by the different Z scalings of the two contributions. The background scales as Z^8 and the cascade term, given by $2p_{3/2} \rightarrow 2s_{1/2} \rightarrow 1s_{1/2}$, scales as Z^{10}. The dash-dotted (decay rate of $2p_{1/2}$-$1s_{1/2}$) and dotted lines are almost coincident in low-Z region and diverge from about $Z=40$, which is evidence of the relativistic effects in the $np_{1/2}$ and $np_{3/2}$.

In Table IX we report two-photon total decay rates for transitions from initial level with $n_i=3$, obtained in the LPA considering the most relevant multipole combinations in Eq. (20). The results of Tung *et al.* [34], presented in this table, were calculated using the analytical formulas described in Ref. [34], which were obtained through the so-called implicit technique that describes the intermediate states by a differential equation. We restrict ourselves to listing the two-photon decay rates obtained in the LPA because in some cases they are very different from the TLA ones when the cascade term in Eq. (35) dominates.

One important aspect concerning total decay rates of resonant transitions is the calculation of the nonresonant decay rate without interference from resonant intermediate states. Cresser *et al.* [39], using a fourth-order perturbation term development, obtained an expression similar to Eq. (35.21) of Ref. [24], where the sum over the intermediate states considers only the states above the initial one, avoiding in this way the resonant denominators, and found the value of 8.2197 s^{-1} for the $3s_{1/2} \rightarrow 1s_{1/2}$ transition rate. Florescu [40], using the same procedure, obtained the value of 8.225 81 s^{-1}. The nonrelativistic limit of Eq. (3) in the Coulomb gauge gives the same expression as the one reported by Cresser *et al.* [39] and, consequently, the same result.

Jentschura *et al.* [41] pointed out that the procedure of Cresser *et al.* [39] is not gauge invariant since in a second-order evaluation the sum over the complete spectrum of intermediate states is required to have equivalence between two different gauges. (More details are given in the appendix of Ref. [19].)

Chluba and Sunyaev [42] developed another method to isolate the nonresonant contribution. In their method, the

TABLE IV. Radiative corrections for several states in a.u.

	$2s_{1/2}$	$2p_{1/2}$	$2p_{3/2}$	$3s_{1/2}$	$3p_{1/2}$	$3p_{3/2}$
			$Z=1$			
Re[SE]+VP$=\Delta E_n$	1.5867×10^{-7}	-1.9542×10^{-9}	1.9095×10^{-9}	4.7376×10^{-8}	-5.5003×10^{-10}	6.4103×10^{-10}
Im[SE]$=\Gamma_n/2$	1.9905×10^{-16}	1.5162×10^{-8}	1.5162×10^{-8}	1.5281×10^{-10}	4.5911×10^{-9}	4.5911×10^{-9}
			$Z=40$			
	$2s_{1/2}$	$2p_{1/2}$	$2p_{3/2}$	$3s_{1/2}$	$3p_{1/2}$	$3p_{3/2}$
Re[SE]+VP$=\Delta E_n$	8.6991×10^{-2}	-1.4913×10^{-3}	7.0905×10^{-3}	2.6401×10^{-2}	-1.3587×10^{-4}	2.3058×10^{-3}
Im[SE]$=\Gamma_n/2$	1.4690×10^{-6}	3.9208×10^{-2}	3.8037×10^{-2}	4.6373×10^{-4}	1.1689×10^{-2}	1.1627×10^{-2}
			$Z=92$			
	$2s_{1/2}$	$2p_{1/2}$	$2p_{3/2}$	$3s_{1/2}$	$3p_{1/2}$	$3p_{3/2}$
Re[SE]+VP$=\Delta E_n$	1.7995	2.4965×10^{-1}	3.2252×10^{-1}	5.7911×10^{-1}	9.3654×10^{-2}	1.1027×10^{-1}
Im[SE]$=\Gamma_n/2$	4.7468×10^{-3}	1.1417	9.5531×10^{-1}	2.7061×10^{-2}	3.1125×10^{-1}	3.0444×10^{-1}

sum over all the intermediate states is split up into resonant and nonresonant states. Although one can make conclusions for the difference between a pure cascade process, i.e., considering only the resonant states with a Lorentzian profile,

TABLE V. Sums of the terms $\mathfrak{h}^{\mathrm{LPA}}$ and $\mathfrak{h}_1^{\mathrm{LPA}}$, given by Eqs. (28) and (30), respectively, for transitions from bound states with $n_i=3$. These values were obtained using the radiative corrections in Table IV and $q=1$.

			$Z=1$		
			i		
f	$3s_{1/2}$	$3p_{1/2}$	$3p_{3/2}$	$3d_{3/2}$	$3d_{5/2}$
$1s_{1/2}$	2.342758	3.966941×10^{-6}	3.230044×10^{-6}	3.706845	3.706854
$2s_{1/2}$	6.452435×10^{-2}	4.925801×10^{-8}	4.926319×10^{-8}	7.762447×10^{-4}	7.750004×10^{-4}
$2p_{1/2}$	2.894796×10^{-8}	4.660148×10^{-2}	4.414498×10^{-4}	3.890718×10^{-8}	3.049476×10^{-9}
$2p_{3/2}$	5.789457×10^{-8}	8.832671×10^{-4}	4.704893×10^{-2}	1.326766×10^{-8}	4.912187×10^{-8}
			$Z=40$		
			i		
f	$3s_{1/2}$	$3p_{1/2}$	$3p_{3/2}$	$3d_{3/2}$	$3d_{5/2}$
$1s_{1/2}$	7.813052×10^{9}	2.872804×10^{7}	2.002016×10^{7}	1.436349×10^{10}	1.441446×10^{10}
$2s_{1/2}$	2.247363×10^{8}	2.812583×10^{5}	3.395829×10^{5}	6.369235×10^{6}	-1.183514×10^{6}
$2p_{1/2}$	1.756667×10^{5}	1.797278×10^{8}	3.117290×10^{6}	3.012475×10^{5}	2.478360×10^{4}
$2p_{3/2}$	3.370367×10^{5}	8.545466×10^{6}	2.168435×10^{8}	8.878266×10^{4}	3.231816×10^{5}
			$Z=92$		
			i		
f	$3s_{1/2}$	$3p_{1/2}$	$3p_{3/2}$	$3d_{3/2}$	$3d_{5/2}$
$1s_{1/2}$	-5.316586×10^{10}	3.647738×10^{10}	2.048248×10^{11}	1.646524×10^{12}	1.637676×10^{12}
$2s_{1/2}$	7.443297×10^{9}	1.683735×10^{8}	6.928218×10^{8}	1.135193×10^{10}	6.013487×10^{9}
$2p_{1/2}$	9.548939×10^{7}	2.314262×10^{10}	3.637390×10^{9}	4.841719×10^{8}	1.534768×10^{7}
$2p_{3/2}$	1.554405×10^{8}	5.312377×10^{9}	5.376493×10^{10}	1.660640×10^{8}	3.122434×10^{8}

TABLE VI. Sums of the terms $\mathfrak{h}^{\mathrm{TLA}}$ and $\mathfrak{h}_1^{\mathrm{TLA}}$, given by Eqs. (37) and (36), respectively, for transitions from bound states with $n_i=3$. These values were obtained without radiative corrections, using $q=10^{-2}$ and following the approach of Jentschura [22].

			$Z=1$		
			i		
f	$3s_{1/2}$	$3p_{1/2}$	$3p_{3/2}$	$3d_{3/2}$	$3d_{5/2}$
$1s_{1/2}$	2.342751	3.966941×10^{-6}	3.230044×10^{-6}	3.706845	3.706854
$2s_{1/2}$	6.452428×10^{-2}	4.925765×10^{-8}	4.926337×10^{-8}	7.762447×10^{-4}	7.750004×10^{-4}
$2p_{1/2}$	2.894793×10^{-8}	4.660148×10^{-2}	4.414498×10^{-4}	3.890718×10^{-8}	3.049476×10^{-9}
$2p_{3/2}$	5.789453×10^{-8}	8.832670×10^{-4}	4.704892×10^{-2}	1.326766×10^{-8}	4.912188×10^{-8}
			$Z=40$		
			i		
f	$3s_{1/2}$	$3p_{1/2}$	$3p_{3/2}$	$3d_{3/2}$	$3d_{5/2}$
$1s_{1/2}$	7.799875×10^{9}	2.872822×10^{7}	2.000453×10^{7}	1.436350×10^{10}	1.441394×10^{10}
$2s_{1/2}$	2.246945×10^{8}	2.802618×10^{5}	3.400453×10^{5}	6.369529×10^{6}	-1.180529×10^{6}
$2p_{1/2}$	1.756241×10^{5}	1.797280×10^{8}	3.116223×10^{6}	3.080467×10^{5}	2.477876×10^{4}
$2p_{3/2}$	3.369973×10^{5}	8.514049×10^{6}	2.167575×10^{8}	8.872957×10^{4}	3.233897×10^{5}
			$Z=92$		
			i		
f	$3s_{1/2}$	$3p_{1/2}$	$3p_{3/2}$	$3d_{3/2}$	$3d_{5/2}$
$1s_{1/2}$	-5.843073×10^{10}	3.632557×10^{10}	2.037502×10^{11}	1.648325×10^{12}	1.637187×10^{12}
$2s_{1/2}$	7.703355×10^{9}	1.624996×10^{8}	7.340967×10^{8}	1.135843×10^{10}	6.400342×10^{9}
$2p_{1/2}$	9.552389×10^{7}	2.313307×10^{10}	3.630875×10^{9}	4.857978×10^{8}	1.528289×10^{7}
$2p_{3/2}$	1.556356×10^{8}	5.270175×10^{9}	5.351656×10^{10}	1.655470×10^{8}	3.134378×10^{8}

and the two-photon emission given by all intermediate states (resonant and nonresonant), the definition of a nonresonant two-photon emission is unclear from the physical point of view.

The values listed in Table VI were used to calculate the nonresonant radiative corrections presented in Table X (setting $q=10^{-3}$). We notice that for the $3s_{1/2}\rightarrow1s_{1/2}$ transition the values calculated in this work differ from the values obtained by Jentschura [22] by 0.01% for $Z=1$ and 0.1% for $Z=40$.

TABLE VII. Same as Table I for the transition $2p_{3/2}\rightarrow1s_{1/2}$.

	Contribution (s^{-1})		
MP	$Z=1$	$Z=40$	$Z=92$
$E1M1$	9.700994×10^{-6}	3.547078×10^{8}	2.938208×10^{12}
$E1E2$	6.612242×10^{-6}	4.597372×10^{7}	1.113120×10^{11}
$E1M3$	1.761532×10^{-16}	3.264236×10^{3}	1.216566×10^{8}
$M1M2$	2.450145×10^{-15}	4.265433×10^{4}	1.129082×10^{9}
$E2M2$	7.227055×10^{-17}	1.337970×10^{3}	4.923824×10^{7}
$E2E3$	4.096369×10^{-18}	7.718214×10^{1}	1.216566×10^{8}
Total	1.631323×10^{-5}	4.007255×10^{8}	3.050699×10^{12}

The reason for some values in Table X being negative, such as the $3s_{1/2}\rightarrow1s_{1/2}$ transition correction for $Z=92$, is due to the evaluation of the two-loop self-energy, which can be negative as any negative correction to the decay rates [22]. In Fig. 8, we represent the values of the nonresonant radiative correction for several values of atomic number.

IV. CONCLUSIONS

By applying a finite basis set constructed from B splines to solve the Dirac equation, we have been able to calculate

TABLE VIII. Same as Table I for the transition $3s_{1/2}\rightarrow2s_{1/2}$.

	Contribution (s^{-1})		
MP	$Z=1$	$Z=40$	$Z=92$
$2E1$	6.452436×10^{-2}	3.167606×10^{8}	1.850546×10^{12}
$E1M2$	6.725935×10^{-14}	1.150220×10^{3}	3.359725×10^{8}
$2M1$	1.038556×10^{-14}	1.241685×10^{2}	1.031596×10^{6}
$2E2$	1.456030×10^{-14}	1.584123×10^{2}	8.482772×10^{5}
$2M2$	1.901242×10^{-27}	6.068107×10^{-5}	4.479357×10^{3}
Total	6.452436×10^{-2}	3.167620×10^{8}	1.85088×10^{12}

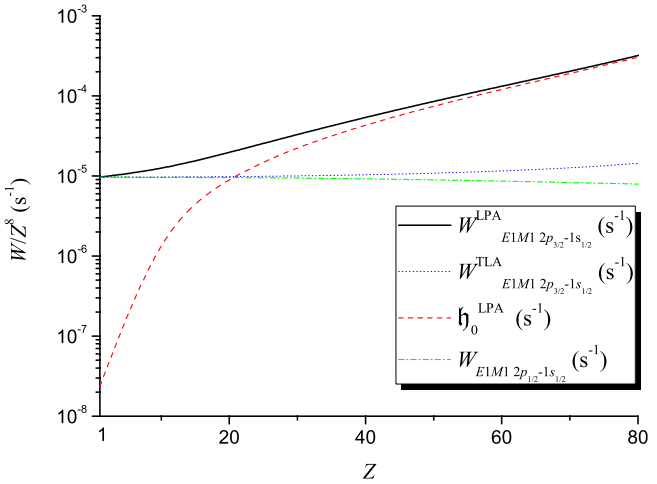

FIG. 7. (Color online) Multipole combination $E1M1$ decay rate values W_{E1M1}, obtained in the LPA and TLA, as functions of the atomic number Z for the transitions $2p_{1/2} \rightarrow 1s_{1/2}$ (dot-dashed line) and $2p_{3/2} \rightarrow 1s_{1/2}$ (solid and dotted lines). The cascade term in LPA is represented by the dashed line.

the decay rates in the line profile and QED based on the two-loop self-energy approaches for all two-photon transitions from initial states with $n=2$ and 3 for a set of hydrogenlike ions with nuclear charge ranging from $Z=1$ to $Z=92$. In these calculations the most significant multipoles contributions were considered, such as the $2E1$, $E1M1$, and $2M1$. We have also studied the spectral distributions of several transitions, which exhibit specific structures, such as resonances and transparencies. The latter reveal that two-photon emission is not possible at certain frequencies. The numerical results obtained in this work are in good agreement with other nonrelativistic and relativistic theoretical results.

The QED approach gives a better contribution for a pure coherent nonresonant two-photon emission than the methods of Cresser *et al.* [39] and Chluba and Sunyaev [42], not only because it is derived from physical arguments, but also due to the fact that it can be obtained from the line profile approach by removing the cascade process and setting the radiative corrections to zero. Therefore, it is a useful technique in theoretical evaluations that require a coherent two-photon

TABLE IX. Total two-photon decay rates (s^{-1}) in the LPA, given by Eq. (20), for transitions from bound states with $n_i=3$.

Total decay rate (s^{-1})					
			$Z=1$		
			i		
f	$3s_{1/2}$	$3p_{1/2}$	$3p_{3/2}$	$3d_{3/2}$	$3d_{5/2}$
$1s_{1/2}$	6.382020×10^{6}	3.431055×10^{1}	3.431043×10^{1}	7.213121×10^{7}	7.212970×10^{7}
$2s_{1/2}$	6.452436×10^{-2}	4.925806×10^{-8}	4.965339×10^{-8}	7.762774×10^{-4}	7.751032×10^{-4}
	6.4527×10^{-2} [a]			7.7589×10^{-4} [a]	
$2p_{1/2}$	2.894796×10^{-8}	4.6601485×10^{-2}	4.414514×10^{-4}	3.890719×10^{-8}	3.070354×10^{-9}
		4.7484×10^{-2} [a]			
$2p_{3/2}$	5.789457×10^{-8}	8.832671×10^{-4}	4.704893×10^{-2}	1.326768×10^{-8}	4.912603×10^{-8}
			$Z=40$		
			i		
f	$3s_{1/2}$	$3p_{1/2}$	$3p_{3/2}$	$3d_{3/2}$	$3d_{5/2}$
$1s_{1/2}$	1.940069×10^{13}	1.465902×10^{11}	1.459393×10^{13}	1.909365×10^{14}	1.846466×10^{14}
$2s_{1/2}$	3.167620×10^{8}	1.249212×10^{6}	6.204266×10^{6}	4.239616×10^{8}	1.256275×10^{9}
$2p_{1/2}$	2.488771×10^{5}	1.797286×10^{8}	2.342989×10^{7}	4.767668×10^{5}	1.268419×10^{6}
$2p_{3/2}$	3.370367×10^{5}	8.545466×10^{6}	2.648671×10^{8}	4.278490×10^{5}	3.734221×10^{5}
			$Z=92$		
			i		
f	$3s_{1/2}$	$3p_{1/2}$	$3p_{3/2}$	$3d_{3/2}$	$3d_{5/2}$
$1s_{1/2}$	1.067206×10^{15}	5.649957×10^{13}	4.187334×10^{13}	6.170663×10^{15}	5.175621×10^{15}
$2s_{1/2}$	1.850884×10^{12}	4.581582×10^{10}	1.219838×10^{11}	5.062691×10^{12}	1.123469×10^{13}
$2p_{1/2}$	8.893987×10^{9}	2.336202×10^{10}	2.576780×10^{11}	9.697069×10^{9}	5.543826×10^{10}
$2p_{3/2}$	1.554405×10^{8}	5.312377×10^{9}	1.059702×10^{12}	1.959473×10^{10}	1.239531×10^{9}

[a]Tung *et al.* [34].

TABLE X. Total nonresonant two-photon corrections (s^{-1}) in the TLA, given by Eq. (20), for transitions from bound states with $n_i=3$ and comparison between the values obtained in this work and other theoretical values.

Total nonresonant correction (s^{-1})					
			$Z=1$		
			i		
f	$3s_{1/2}$	$3p_{1/2}$	$3p_{3/2}$	$3d_{3/2}$	$3d_{5/2}$
$1s_{1/2}$	2.082562	2.981766×10^{-6}	2.98676×10^{-6}	1.042768	1.042835
	2.082853[a]			1.042896[b]	
$2s_{1/2}$	6.452428×10^{-2}	4.925721×10^{-8}	4.926293×10^{-8}	7.762407×10^{-4}	7.749962×10^{-4}
	6.4530×10^{-2} [a]				
$2p_{1/2}$	2.894793×10^{-8}	4.6601486×10^{-2}	4.414498×10^{-4}	3.890718×10^{-8}	3.049476×10^{-9}
$2p_{3/2}$	5.789453×10^{-8}	8.832670×10^{-4}	4.704892×10^{-2}	1.326767×10^{-8}	4.912188×10^{-8}
			$Z=40$		
			i		
f	$3s_{1/2}$	$3p_{1/2}$	$3p_{3/2}$	$3d_{3/2}$	$3d_{5/2}$
$1s_{1/2}$	6.560351×10^{9}	2.224659×10^{7}	1.885681×10^{7}	3.456276×10^{9}	3.874677×10^{9}
$1s_{1/2}$	6.554×10^{9} [c]				
$2s_{1/2}$	2.245669×10^{8}	2.793230×10^{5}	3.395425×10^{5}	5.920457×10^{6}	-2.764917×10^{6}
$2p_{1/2}$	1.755215×10^{5}	1.797280×10^{8}	3.088316×10^{6}	3.078375×10^{5}	2.349043×10^{4}
$2p_{3/2}$	3.369973×10^{5}	8.514049×10^{6}	2.166915×10^{8}	8.842254×10^{4}	3.233689×10^{5}
			$Z=92$		
			i		
f	$3s_{1/2}$	$3p_{1/2}$	$3p_{3/2}$	$3d_{3/2}$	$3d_{5/2}$
$1s_{1/2}$	-3.842113×10^{11}	2.891626×10^{10}	7.976296×10^{10}	8.916260×10^{10}	3.271857×10^{11}
$2s_{1/2}$	5.570205×10^{9}	1.258571×10^{8}	7.132981×10^{8}	7.613467×10^{9}	-5.085413×10^{9}
$2p_{1/2}$	8.535648×10^{7}	2.313315×10^{10}	3.386706×10^{9}	4.767493×10^{8}	-5.866950×10^{7}
$2p_{3/2}$	1.556356×10^{8}	5.270175×10^{9}	5.253150×10^{10}	1.539227×10^{8}	3.127867×10^{8}

[a]Jentschura [22].
[b]Jentschura [46].
[c]Jentschura and Surzhykov [23].

decay rate rather than the sum of this term along with the sequential one-photon decay rate (cascade process).

We conclude that the line profile approach is the most suitable for comparison with experimental results since it includes the terms associated with cascade process as well as radiative corrections.

We end this conclusion by emphasizing that the method of integration used to obtain one-electron decay rates (in both approaches and for both nonresonant and resonant transitions) can be adapted perfectly to ions with two or three electrons.

ACKNOWLEDGMENTS

This research was supported in part by FCT Projects No. POCTI/FAT/44279/2002 and No. POCTI/0303/2003 (Portugal), financed by the European Community Fund FEDER, by the French-Portuguese collaboration (PESSOA Program, Contract No. 441.00), and by the Acções Integradas Luso-Francesas (Contract No. F-11/09). The work of A.S. was supported by the Helmholtz Gemeinschaft (Nachwuchsgruppe VH-NG-421). Laboratoire Kastler Brossel is "Unité Mixer de Recherche du CNRS, de l' ENS et de l'UPMC No. 8552." P.I. acknowledges the support of the Helmholtz Allianz Program of the Helmholtz Association, under Contract No. HA-216, "Extremes of Density and Temperature: Cosmic Matter in the Laboratory." P.A. acknowledges the support of the FCT, under Contract No. SFRH/BD/37404/2007.

APPENDIX

In order to make the task of deriving the matrix elements less cumbersome, further simplifications can be done in the

TABLE XI. Values of the coefficients a_0^j (s^{-2}) and a_1^j (s^{-1}), given by Eq. (26), of the transition $3s_{1/2} \rightarrow 1s_{1/2}$ for several values of Z.

	$Z=1$	$Z=40$	$Z=92$
$a_0^{1/2}$	5.081524×10^{-3}	3.554138×10^{10}	3.793201×10^{13}
$a_1^{1/2}$	-3.468385×10^{-1}	-1.425932×10^{9}	-2.066515×10^{11}
$a_0^{3/2}$	1.016398×10^{-2}	8.148532×10^{10}	1.250476×10^{14}
$a_1^{3/2}$	-6.936930×10^{-1}	-2.929768×10^{9}	-3.488011×10^{11}

matrix elements [Eqs. (14) and (16)] by noticing that the longitudinal part of the operator $\tilde{a}_{LM}^{(\lambda)}$ [43],

$$(\tilde{a}_{LM}^{(-1)})_{\parallel} = \frac{c}{i\omega}\alpha \cdot \nabla \phi_{L,M}, \tag{A1}$$

can be written using a commutation relation as

$$(\tilde{a}_{LM}^{(-1)})_{\parallel} = \frac{c}{i\omega}[H_D, \phi_{L,M}], \tag{A2}$$

where H_D stands for the Dirac Hamiltonian and $\phi_{L,M}$ are the components of the spherical tensor of rank L resulting from the multipole expansion of the potential A_j^*. The reduction of Eq. (A2) to radial integrals along with the scalar term of the potential A_j^* leads to the following expression for the radial element matrix $\bar{M}_{f,i}^{(-1,L)}$:

$$\bar{M}_{f,i}^{(-1,L)} = G(2L+1)\left(\frac{\omega+\omega_{fi}}{\omega}\right)J^{(L)}, \tag{A3}$$

where ω_{fi} is the energy of the one-photon transition. This term is gauge independent for one photon, as demonstrated by Grant [25], since $\omega_{fi}=-\omega$. Considering Eq. (A2), the radial matrix element $\bar{M}_{f,i}^{(1,L)}$ can also be rewritten as

$$\bar{M}_{f,i}^{(1,L)} = \frac{(2L+1)}{\sqrt{L(L+1)}}\left[-(\kappa_f-\kappa_i)I_{L-1}^{+} + LI_{L-1}^{-} + L\frac{\omega_{fi}}{\omega}J^L\right]. \tag{A4}$$

The explicit expressions of the derivatives of the matrix elements [Eqs. (A4), (15), and (A3)] are given by

$$\frac{d}{d\omega}[\bar{M}_{f,i}^{(1,L)}(\omega)] = \frac{2L+1}{\sqrt{L(L+1)}}\left[(\kappa_f-\kappa_i)\left(I_L^R + \frac{I_{L-1}^{+}}{\omega}\right) - L\frac{I_{L-1}^{-}}{\omega} - \frac{\omega_{fi}}{\omega^2}L(L+2)J^{(L)}\right], \tag{A5}$$

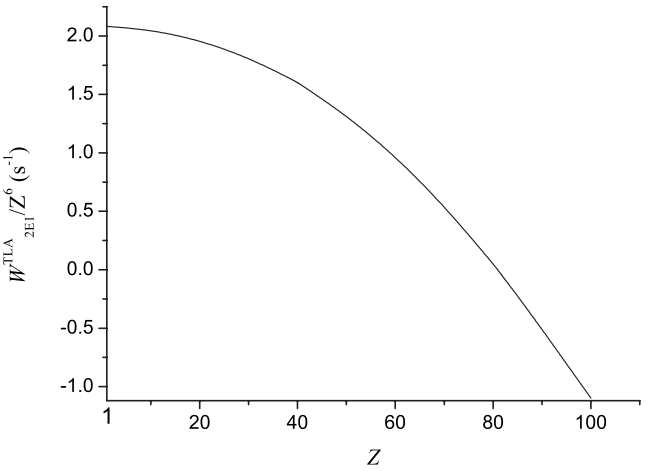

FIG. 8. Nonresonant correction of the multipole combination $2E1$ in the $3s_{1/2} \rightarrow 1s_{1/2}$ transition divided by Z^6 as function of the atomic number Z.

$$\frac{d}{d\omega}[\bar{M}_{f,i}^{(0,L)}(\omega)] = \frac{2L+1}{\sqrt{L(L+1)}}(\kappa_f+\kappa_i)\left[I_{L-1}^R - \frac{(L+1)}{\omega}I_L^{+}\right], \tag{A6}$$

and

$$\frac{d}{d\omega}[\bar{M}_{f,i}^{(-1,L)}(\omega)] = G(2L+1)\left\{\left(\frac{\omega+\omega_{fi}}{\omega}\right)J_R^{(L-1)} - \frac{1}{\omega^2}[(L+1)\omega + (L+2)\omega_{fi}]J^{(L)}\right\}, \tag{A7}$$

where the integrals $J_R^{(L)}$ and I_L^R are defined by

$$I_L^R = \frac{1}{c}\int_0^\infty (P_fQ_i + P_iQ_f)rj_L\left(\frac{\omega r}{c}\right)dr, \tag{A8}$$

$$J_R^{(L)} = \frac{1}{c}\int_0^\infty (P_fP_i + Q_fQ_i)rj_L\left(\frac{\omega r}{c}\right)dr. \tag{A9}$$

Using these expressions, along with the definitions given by Eq. (26), we were able to obtain the coefficients a_0^j and a_1^j listed in Table XI for the transition $3s_{1/2} \rightarrow 1s_{1/2}$ for ions with $Z=1$, 40, and 92.

[1] M. Göppert-Mayer, Ann. Phys. **401**, 273 (1931).
[2] L. Spitzer and J. L. Greenstein, Astrophys. J. **114**, 407 (1951).
[3] S. Seager, D. D. Sasselov, and D. Scott, Astrophys. J. **523**, L1 (1999).
[4] J. Chluba and R. A. Sunyaev, Astron. Astrophys. **446**, 39 (2006).
[5] C. Schwob, L. Jozefowski, B. de Beauvoir, L. Hilico, F. Nez, L. Julien, F. Biraben, O. Acef, J. J. Zondy, and A. Clairon, Phys. Rev. Lett. **82**, 4960 (1999).
[6] B. de Beauvoir, C. Schwob, O. Acef, L. Jozefowski, L. Hilico, F. Nez, L. Julien, A. Clairon, and F. Biraben, Eur. Phys. J. D **12**, 61 (2000).

[7] T. W. Hänsch, Rev. Mod. Phys. **78**, 1297 (2006).
[8] H. Gould and R. Marrus, Phys. Rev. A **28**, 2001 (1983).
[9] W. Perrie, A. J. Duncan, H. J. Beyer, and H. Kleinpoppen, Phys. Rev. Lett. **54**, 1790 (1985).
[10] T. Tsujibayashi, M. Itoh, J. Azuma, M. Watanabe, O. Arimoto, S. Nakanishi, H. Itoh, and M. Kamada, Phys. Rev. Lett. **94**, 076401 (2005).
[11] P. T. C. So, C. Y. Dong, and B. R. Masters, in *Biomedical Photonics Handbook*, edited by T. Vo-Dinh (CRC Press LLC, Boca Raton, 2003).
[12] S. Fujiyoshi, M. Fujiwara, and M. Matsushita, Phys. Rev. Lett. **100**, 168101 (2008).
[13] E. G. Drukarev and A. N. Moskalev, Zh. Eksp. Teor. Fiz. **73**, 2060 (1977).
[14] M. Maul, A. Schäfer, W. Greiner, and P. Indelicato, Phys. Rev. A **53**, 3915 (1996).
[15] E. Lamour, C. Prigent, B. Eberhardt, J. P. Rozet, and D. Vernhet, Rev. Sci. Instrum. **80**, 023103 (2009).
[16] J. P. Santos, F. Parente, and P. Indelicato, Eur. Phys. J. D **3**, 43 (1998).
[17] A. Surzhykov, P. Koval, and S. Fritzsche, Phys. Rev. A **71**, 022509 (2005).
[18] L. N. Labzowsky, A. V. Shonin, and D. A. Solovyev, J. Phys. B **38**, 265 (2005).
[19] S. P. Goldman and G. W. F. Drake, Phys. Rev. A **24**, 183 (1981).
[20] H. M. T. Nganso and M. G. K. Njock, J. Phys. B **40**, 807 (2007).
[21] L. N. Labzowsky and A. V. Shonin, Phys. Rev. A **69**, 012503 (2004).
[22] U. D. Jentschura, J. Phys. A: Math. Theor. **40**, F223 (2007).
[23] U. D. Jentschura and A. Surzhykov, Phys. Rev. A **77**, 042507 (2008).
[24] A. I. Akhiezer and V. B. Berestetskii, *Quantum Electrodynamics* (Interscience, New York, 1965).
[25] I. P. Grant, J. Phys. B **7**, 1458 (1974).
[26] R. W. Dunford, E. P. Kanter, B. Krässig, S. H. Southworth, L. Young, P. H. Mokler, and T. Stöhlker, Phys. Rev. A **67**, 054501 (2003).
[27] F. Low, Phys. Rev. **88**, 53 (1952).
[28] O. Y. Andreev, L. N. Labzowsky, G. Plunien, and D. A. Solovyev, Phys. Rep. **455**, 135 (2008).
[29] H. R. Rosner and C. P. Bhalla, Z. Phys. **231**, 347 (1970).
[30] P. Indelicato, Phys. Rev. A **51**, 1132 (1995).
[31] W. R. Johnson, S. A. Blundell, and J. Sapirstein, Phys. Rev. A **37**, 307 (1988).
[32] L. Labzowsky, D. Solovyev, G. Plunien, and G. Soff, Eur. Phys. J. D **37**, 335 (2006).
[33] P. J. Mohr and B. N. Taylor, Rev. Mod. Phys. **77**, 1 (2005).
[34] J. H. Tung, X. M. Ye, G. J. Salamo, and F. T. Chan, Phys. Rev. A **30**, 1175 (1984).
[35] J. H. Tung, A. Z. Tang, G. J. Salamo, and F. T. Chan, J. Opt. Soc. Am. B **3**, 837 (1986).
[36] O. Gorceix, P. Indelicato, and J. P. Desclaux, J. Phys. B **20**, 639 (1987).
[37] P. Indelicato, Nucl. Instrum. Methods Phys. Res. B **31**, 14 (1988).
[38] J. P. Desclaux, Comput. Phys. Commun. **9**, 31 (1975).
[39] J. D. Cresser, A. Z. Tang, G. J. Salamo, and F. T. Chan, Phys. Rev. A **33**, 1677 (1986).
[40] V. Florescu, I. Schneider, and I. N. Mihailescu, Phys. Rev. A **38**, 2189 (1988).
[41] U. D. Jentschura, J. Evers, C. H. Keitel, and K. Pachucki, New J. Phys. **4**, 49 (2002).
[42] J. Chluba and R. A. Sunyaev, Astron. Astrophys. **480**, 629 (2008).
[43] D. M. Brink and G. R. Satchler, *Angular Momentum* (Clarendon, New York, 1994).
[44] V. Florescu, S. Patrascu, and O. Stoican, Phys. Rev. A **36**, 2155 (1987).
[45] A. Quattropani, F. Bassani, and S. Carillo, Phys. Rev. A **25**, 3079 (1982).
[46] U. D. Jentschura, J. Phys. A: Math. Theor. **41**, 155307 (2008).